The Journal of Immunology

Depletion of Plasmacytoid Dendritic Cells Inhibits Tumor Growth and Prevents Bone Metastasis of Breast Cancer Cells

Anandi Sawant, Jonathan A. Hensel, Diptiman Chanda, Brittney A. Harris, Gene P. Siegal, Akhil Maheshwari and Selvarangan Ponnazhagan

J Immunol 2012; 189:4258-4265; Prepublished online 26 September 2012;
doi: 10.4049/jimmunol.1101855
http://www.jimmunol.org/content/189/9/4258

The Journal of Immunology is published twice each month by
The American Association of Immunologists, Inc.,
1451 Rockville Pike, Suite 650, Rockville, MD 20852

Print ISSN: 0022-1767 Online ISSN: 1550-6606.

Depletion of Plasmacytoid Dendritic Cells Inhibits Tumor Growth and Prevents Bone Metastasis of Breast Cancer Cells

Anandi Sawant,* Jonathan A. Hensel,*,[1] Diptiman Chanda,* Brittney A. Harris,* Gene P. Siegal,* Akhil Maheshwari,[†,2] and Selvarangan Ponnazhagan*

Elevated levels of plasmacytoid dendritic cells (pDC) have been reported in breast cancer patients, but the significance remains undefined. Using three immunocompetent mouse models of breast cancer bone metastasis, we identified a key role for pDC in facilitating tumor growth through immunosuppression and aggressive osteolysis. Following infiltration of macrophages upon breast cancer dissemination, there was a steady increase in pDC within the bone, which resulted in a sustained Th2 response along with elevated levels of regulatory T cells and myeloid-derived suppressor cells. Subsequently, pDC and $CD4^+$ T cells, producing osteolytic cytokines, increased with tumor burden, causing severe bone damage. Microcomputed tomography and histology analyses of bone showed destruction of femur and tibia. The therapeutic significance of this finding was confirmed by depletion of pDC, which resulted in decreased tumor burden and bone loss by activating tumor-specific cytolytic $CD8^+$ T cells and decreasing suppressor cell populations. Thus, pDC depletion may offer a novel adjuvant strategy to therapeutically influence breast cancer bone metastasis. *The Journal of Immunology*, **2012, 189: 4258–4265.**

Nearly 80–90% of breast cancer patients with advanced disease have osteolytic disease, characterized by increased bone damage resulting from enhanced osteoclast activity (1). The presence of such bone lesions usually signifies serious morbidity and a grave prognosis, with severe pain, pathological fractures, nerve compression syndromes, and hypercalcemia (2). Current therapies for bone metastasis in breast cancer patients are limited and are focused only on symptomatic management, limiting the progression of established disease (3). Although a significant amount of research has been carried out on understanding breast cancer bone metastasis, not much is known about the events leading to the bone metastasis. Hence, a better understanding of the molecular mechanisms involved in the formation and progression of bone metastases is needed.

Dissemination of the primary tumor to the bone triggers the production of osteolytic cytokines and growth factors that result in osteoclast activation and the promotion of tumor growth and immune suppression in the bone microenvironment (4). Conversely, products of bone cells are critical for normal development of the hematopoietic and immune systems (4). In osteopenic conditions, such as osteoporosis, bone destruction results from enhanced osteoclast activity with a concomitant decrease in osteoblast numbers, without a significant alteration in the immune system (5). But the osteolytic bone changes observed in bone metastasis are triggered by a coordinated interplay of bone-homing cancer cells, osteoclasts, and the immune cells in the bone marrow (BM) (6). Thus, elucidation of the molecular mechanisms during these interactions should provide new insights into the treatment for cancer bone metastasis.

Using immunocompetent mouse models of breast cancer dissemination to bone and other organs, the current study characterized the immune mechanisms that regulate osteolytic breast cancer metastasis at different stages of tumor progression. Results indicated that the vicious cascade promoting tumor growth, immune suppression, and bone damage is regulated by plasmacytoid dendritic cells (pDC), shifting the Th cell homeostasis greatly toward the Th2 phenotype, independent of the effects of myeloid suppressor cells. Depletion of pDC in vivo resulted in a significant increase in the Th1 response, leading to a decrease in both tumor growth and bone damage. Further, reversal of the Th2 to Th1 response resulted in increased $CD8^+$ T cell activity against the tumor in bone and visceral organs. Collectively, these data indicate the potential of this strategy to decrease bone morbidity and increase survival in advanced-stage breast cancer patients.

Materials and Methods

An in vivo model for breast cancer bone metastasis

Mouse breast cancer cell lines 4T1, constitutively expressing firefly luciferase [4T1(fLuc)], TM40D, and r3T were kind gifts from Dr. Xiaoyuan Chen (Stanford University, Stanford, CA), Dr. Andre Lieber (University of Washington, Seattle, WA), and Dr. Susan Rittling (Forsyth Institute, Cambridge, MA), respectively, and were cultured as described previously (7–9). Approximately 10^5 cells from each cell line were injected via the intracardiac route in syngeneic, female mice at 6–8 wk of age (Frederick Cancer Research and Development Center, Frederick, MD). Progression of 4T1 tumor growth and dissemination to the bone were followed by noninvasive imaging of mice using the IVIS Imaging System (Xenogen). On days 3, 7, 10, and 14, cohorts of mice were sacrificed for analyses. Blood was collected, and serum was separated. Selected visceral organs and bones were collected for histology. Spleen and BM were used for enumerating the

*Department of Pathology, University of Alabama at Birmingham, Birmingham, AL 35294; and [†]Department of Pediatrics, University of Alabama at Birmingham, Birmingham, AL 35294

[1]Current address: Department of Surgery/Urology, University of Colorado, Denver, Denver, CO.

[2]Current address: Department of Pediatrics, University of Illinois, Chicago, IL.

Received for publication June 24, 2011. Accepted for publication August 26, 2012.

This work was supported in part by National Institutes of Health Grants R01AR050251, 1R01AR058344-01, R01CA133737, and P30 AR046031-10 and by U.S. Army Department of Defense Grants BC044440 and BC101411.

Address correspondence and reprint requests to Prof. Selvarangan Ponnazhagan, Department of Pathology, University of Alabama at Birmingham, 1825 University Boulevard, Shelby 814, Birmingham, AL 35294. E-mail address: pons@uab.edu

The online version of this article contains supplemental material.

Abbreviations used in this article: BM, bone marrow; MDSC, myeloid-derived suppressor cell; micro-CT, microcomputed tomography; OPG, osteoprotegerin; pDC, plasmacytoid dendritic cell; TRAP, tartrate-resistant acid phosphatase; Treg, regulatory T cell; UAB, University of Alabama at Birmingham; WT, wild-type.

www.jimmunol.org/cgi/doi/10.4049/jimmunol.1101855

immune cell profile and activation status. Tumor progression was also assessed in an IFN-αR knockout mouse model ($IFNAR^{-/-}$) on a BALB/c background (kindly provided by Dr. Andrew Mellor, Georgia Health Sciences University, Augusta, GA) and on a C57BL/6 background using a syngeneic osteolytic cell line.

Immune cell depletion

To deplete pDC mice were injected i.p. with 250 μg PDCA-1 Ab (clone # JF05-IC2.41; Miltenyi Biotec, Auburn, CA) every other day (10). As a control, mice were injected with similar amounts of IgG Ab (Miltenyi Biotec). Four days after injection of Abs, blood was collected by retinal bleeding. Mononuclear cells, obtained by Ficoll-Hypaque (GE Healthcare, Piscataway, NJ) gradient extraction, were incubated with PDCA-1–Alexa Fluor 647 Ab (eBioscience, San Diego, CA) for 30 min and enumerated by flow cytometry. Once depletion of pDC was confirmed, mice were challenged with 10^5 4T1(fLuc) cells by the intracardiac route. Injection of PDCA-1 or IgG Abs was continued until the end of the experiment.

Microcomputed tomography and histology

Upon sacrifice of tumor-challenged mice at different time points, both femur and tibia were collected and fixed in 4% buffered formalin for 2 d and subjected to microcomputed tomography (micro-CT) analysis (Micro-CT40; SCANCO Medical, Wayne, PA). The formalin-fixed bones were decalcified in 2.5% EDTA (pH 8) for 2 wk. Five-micrometer paraffin-embedded sections were used for histological analysis.

Immunohistochemistry

The presence of breast cancer cells in the visceral tissues and bone was detected by conventional light microscopic evaluation of H&E-stained tissue sections by a senior anatomic pathologist and confirmed by staining with cytokeratin-8 Ab (Abcam, Cambridge, MA), as described previously (11). The presence of osteoclasts within the bone sections was detected by tartrate-resistant acid phosphatase (TRAP) staining, as described previously (12). All of the microscopic images were obtained using a Leica DMI4000B microscope, attached to a Leica DFC500 digital camera. LASv3.6.0 software was used to optimize picture quality and to generate scale bars for individual images.

Isolation of immune cells and FACS analysis

Immune cells were isolated from the bone of tumor-challenged mice. Both femur and tibia were flushed to collect BM cells. Following RBC lysis using ACK lysis buffer (Quality Biologicals, Gaithersburg, MD), cells were suspended in FACS-staining buffer (PBS + 2% FBS + 0.01% sodium azide) and incubated with Fc Block for 15 min at 4˚C. These cells were stained (10^6 cells/group) to detect various immune cell populations using cell-specific fluorescence-conjugated Abs, purchased from eBioscience, for 30 min at 4˚C. Upon fixation with 4% paraformaldehyde, cells were enumerated using a FACSCalibur Flow Cytometer (Beckman Coulter, Hialeah, FL) (13). A total of 30×10^3 events was acquired for each sample. The data were analyzed using FlowJo software. To detect the presence of regulatory T cells (Tregs), cells stained with Abs to CD3 (clone 17A2), CD4 (clone GK1.5), and CD25 (clone PC61.5) were permeabilized with a commercially available permeabilization buffer (eBioscience) for 30 min at 4˚C and then stained with Ab to Foxp3 for 30 min at 4˚C. A subset of $CD25^+Foxp3^+$ cells was detected within the $CD3^+CD4^+$ cells; these cells were considered Tregs.

To detect the presence of PDCA-1 Ag on the 4T1(fLuc) cells, BM cells were collected upon sacrifice of mice with established breast cancer bone metastasis. Following the addition of Fc Block, cells were stained with Abs to CD45 (clone 30-F11) and PDCA-1 (clone eBio927) for 30 min at 4˚C. Cells that stained negative for both of the Abs were sorted, and cell lysate was prepared. Luciferase assay was carried out per the manufacturer's instructions (Promega). As a control, 4T1(fLuc) cells grown in vitro were used for the luciferase assay.

Coculture assay for osteoclast activity

For isolation of monocytes, cells were incubated with biotinylated CD115 Ab (eBioscience) for 15 min at 4˚C, followed by incubation with anti-biotin microbeads (Miltenyi Biotec). Magnetic separation was carried out per the manufacturer's instructions. A commercially available kit was used for isolation of $CD4^+$ T cells (Miltenyi Biotec). Monocytes and $CD4^+$ T cells were cultured at a ratio of 1:100; monocytes were plated in 96-well tissue culture plates (Corning, Corning, NY), and $CD4^+$ T cells were placed in 0.2-μm tissue culture inserts (Nalge Nunc International, Rochester, NY). Media were changed as described previously (14). To determine the role of RANKL and IL-15 in osteoclast generation, recombinant osteoprotegerin (OPG; 100 ng/ml) or IL-15 Ab (10 μg/ml) was added to the coculture either individually or in combination. After 10 d, the presence of osteoclasts was detected by TRAP staining.

Cytokine assay

RNA was isolated from $CD4^+$ T cells by the TRIzol RNA-extraction method (Invitrogen, Carlsbad, CA). cDNA was prepared per the manufacturer's instructions (Bio-Rad, Hercules, CA) and was used in real-time RT-PCR assays for detecting the presence of the cytokines IL-3, IL-6, IL-10, IL-11, IL-12, IL-15, IL-17, TGF-β, and RANKL.

Serum cytokine levels were assayed using a commercially available Mouse 22-plex cytokine assay kit obtained from Millipore (Millipore, Billerica, MA). Each assay was performed in triplicate.

Cytotoxicity assay

$CD8^+$ T cells were isolated from the BM using a commercially available $CD8a^+$ T cell isolation kit II (Miltenyi Biotec) and were used as the effector cells. 4T1(fLuc) cells were used as the target population. The assay was set up with E:T ratios of 5:1, 10:1, 20:1, and 40:1. The cytotoxicity assay was performed using the commercially available LIVE/DEAD cell-mediated cytotoxicity kit (Molecular Probes, Eugene, OR).

Statistical analysis

Data are presented as mean ± SE. Statistical analysis was performed using the Student *t* test. Statistical significance was determined at $p < 0.05$.

Results

An in vivo model of breast cancer bone dissemination

For understanding possible mechanisms that are conducive for the growth of breast cancer in the bone, we used three models with syngeneic breast cancer cell lines: 4T1(fLuc) cells in BALB/c, r3T cells in 129S, and TM40D cells in BALB/c mice. Upon intracardiac injection, these cells readily metastasized to various organs, including the bone (Fig. 1A). Histologic analysis verified the presence of cancer cells in the liver and lungs (Fig. 1B), as well as in the tibia and femur (Fig. 1C). Micro-CT analysis of the tibia and femur, 14 d after tumor challenge, showed a dramatic destruction of bone compared with age-matched controls (Fig. 1D, Supplemental Fig. 1), with increased osteoclast numbers (Fig. 1E).

Dissemination of cancer cells to the bone initiates an inflammatory reaction followed by pDC enrichment

As tumor cells disseminated to the bone, cohorts of mice were sacrificed, and cells were collected from the BM to examine the profile of immune cells mediating the disease pathology. Results indicated that as breast cancer disseminated to the bone, there was an initial macrophage infiltration (Fig. 2A), followed by an increase in the $B220^+CD11c^+$ (clone RA3-6B2 for B220 and clone N418 for CD11c Ab) pDC population (Fig. 2B). To further confirm the presence of pDC, $B220^+CD11c^+$ cells were stained for markers, including Singlec-H (clone eBio440c), PDCA-1, and Gr-1. Close to or >90% of the $B220^+CD11c^+$ cells were positive for these markers, confirming the pDC increase in the bone (Fig. 2C).

Increased pDC numbers with increased bone metastasis were observed in all three models, confirming that elevated pDC numbers during progressive stages of breast cancer dissemination are not due to the variability in the genetic background of the mice used. (Fig. 2D, 2E).

Elevation of pDC numbers is accompanied by skewing of immune response toward Th2

Next, the effect of elevated pDC levels on the T cell immune response was analyzed by characterizing the Th response in BALB/c mice with 4T1(fLuc) cells. The results of this study revealed significantly high levels of IL-4 compared with IFN-γ levels that progressed with tumor growth and bone metastasis, thus indicating

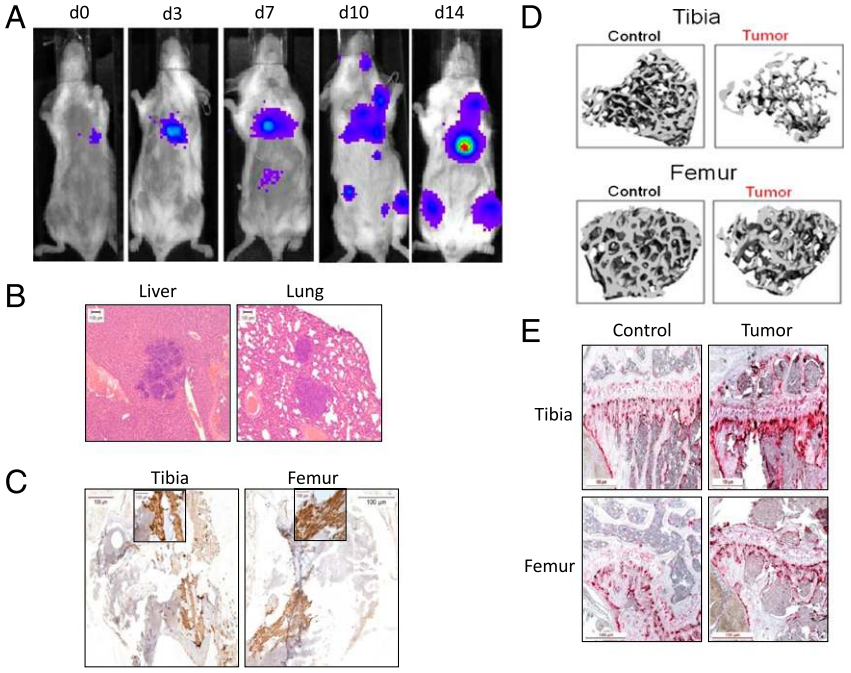

FIGURE 1. In vivo model for bone metastasis of breast cancer. (**A**) The murine breast cancer cell line 4T1(fLuc) was injected into female BALB/c mice via the intracardiac route. Growth and spread of the tumor was followed on days 3, 7, 10, and 14 by noninvasive luciferase imaging. A representative image for each time point is shown. (**B**) Mice were sacrificed, liver and lungs were collected, and paraffin sections were stained with H&E to detect the presence of tumor cells. Representative images from mice sacrificed 14 d posttumor challenge. (**C**) Cytokeratin-8 staining was performed on paraffin sections of the femur and tibia from mice 14 d after tumor challenge (*insets,* original magnification ×40). (**D**) Fourteen days posttumor challenge, tibia and femur were collected and subjected to micro-CT analysis. Tibia and femur from age-matched mice were included as a control. (**E**) Paraffin sections from 14 d posttumor-challenged mice were stained with TRAP to detect osteoclasts. Six mice were used for each time point, and the experiment was performed three times independently. Scale bars, 100 μm.

a skewing toward Th2 response as the cancer progressed to invade and proliferate within the bone (Fig. 3A). The multiplex cytokine analysis from the sera of mice revealed an increased secretion of Th2-specific cytokines (IL-5 and IL-6) and reduced levels of Th1-specific cytokines (IL-12 and IP-10) (data not shown). The switch to a Th2 response also correlated with increased pDC levels.

Because pDC skew the immune response toward a Th2 phenotype via a CD40–CD40L interaction in the presence of IL-3 (15), we examined the surface expression of CD40 (clone 1C10) on pDC and CD40L (clone PC61.5) on $CD4^+$ T cells. The skewing of the immune response toward the Th2 phenotype correlated with increased expression of CD40 and CD40L on pDC and $CD4^+$ T cells, respectively (Fig. 3B). IL-3 levels were elevated in $CD4^+$ T cells (Fig. 3C). Together, these data show that elevated pDC in the bone microenvironment polarizes the immune response toward a suppressive Th2 phenotype that allows tumor growth and spread into bone.

Increased production of osteolytic cytokines leads to increased osteoclast numbers and bone destruction

Cytokine analysis by the multiplex assay using sera from mice indicated a significant increase in the levels of IL-15, RANTES, and MCP-1, known inducers of osteoclasts, as cancer dissemination progressed into and within the bone (Supplemental Fig. 1). Because $CD4^+$ T cells are a major source of osteolytic cytokines, we assayed for the presence of these cytokines in $CD4^+$ T cells from the BM of tumor-challenged mice. Our data indicated significantly higher levels of IL-6, IL-11, and IL-15 with increased bone destruction (Fig. 4A). We next determined whether the increased cytokine production by $CD4^+$ T cells resulted in increased osteoclast numbers. To assay for osteoclast numbers, $CD4^+$ T cells, isolated from either spleen or BM, were cocultured with BM-derived monocytes. The results indicated significantly high numbers of osteoclasts by TRAP staining when monocytes were cocultured with BM-derived $CD4^+$ T cells compared with those from spleen (Fig. 4B). Further, the number of osteoclasts increased as breast cancer metastasized within the bone.

We next determined whether the $CD4^+$ T cells in the BM of tumor-bearing mice are more primed to effect monocyte differentiation into osteoclasts. For this purpose, monocytes from control mice were cocultured with $CD4^+$ T cells from tumor-challenged mice, and monocytes from the tumor-challenged mice were cocultured with $CD4^+$ T cells from control mice. The results indicated a significant increase in osteoclast numbers when $CD4^+$ T cells from tumor-bearing mice were cocultured with monocytes from tumor-challenged mice or from control mice (Fig. 4C). Conversely, $CD4^+$ T cells from control mice induced fewer osteoclasts when cultured with tumor-derived monocytes. However, osteoclast numbers were still significantly greater than that obtained after culturing monocytes and $CD4^+$ T cells from control mice, suggesting that monocytes from tumor-challenged mice are more primed toward osteoclast differentiation.

Further, to determine which osteolytic cytokines played a major role in osteoclast activation, OPG, a soluble decoy receptor of RANKL, and Ab to IL-15 were added to the culture either individually or in combination. The results of this study indicated that the number of osteoclasts was considerably reduced when OPG and IL-15 Abs were added individually or in combination (Fig. 4D), confirming that both RANKL and IL-15 induce monocyte differentiation toward osteoclasts.

Depletion of pDC in vivo results in reduced tumor growth and absence of bone metastasis

To confirm that pDC are key regulators of breast cancer bone metastasis, pDC depletion was performed in vivo with PDCA-1 Ab (Supplemental Fig. 2). As a control, cohorts of mice received isotype IgG Ab. On day 12 posttumor challenge, tumor growth was observed in the bones of both naive (challenged with 4T1 cells but without any Ab treatment) and IgG-injected mice. However, PDCA-1–injected mice showed a dramatic reduction in overall tumor burden (Fig. 5A, 5B), and the tumor cells did not disseminate to bone (Fig. 5A). Metastasis to lungs was significantly less compared with naive and IgG-injected groups (Fig. 5C, 5D). Cytokeratin-8 staining did not reveal the occult presence of cancer cells in the tibia of PDCA-1–injected mice, further supporting the luciferase image analysis (Fig. 5E).

To rule out the possibility that reduced tumor burden in PDCA-1–injected mice was not due to binding of the PDCA-1 Ab to 4T1

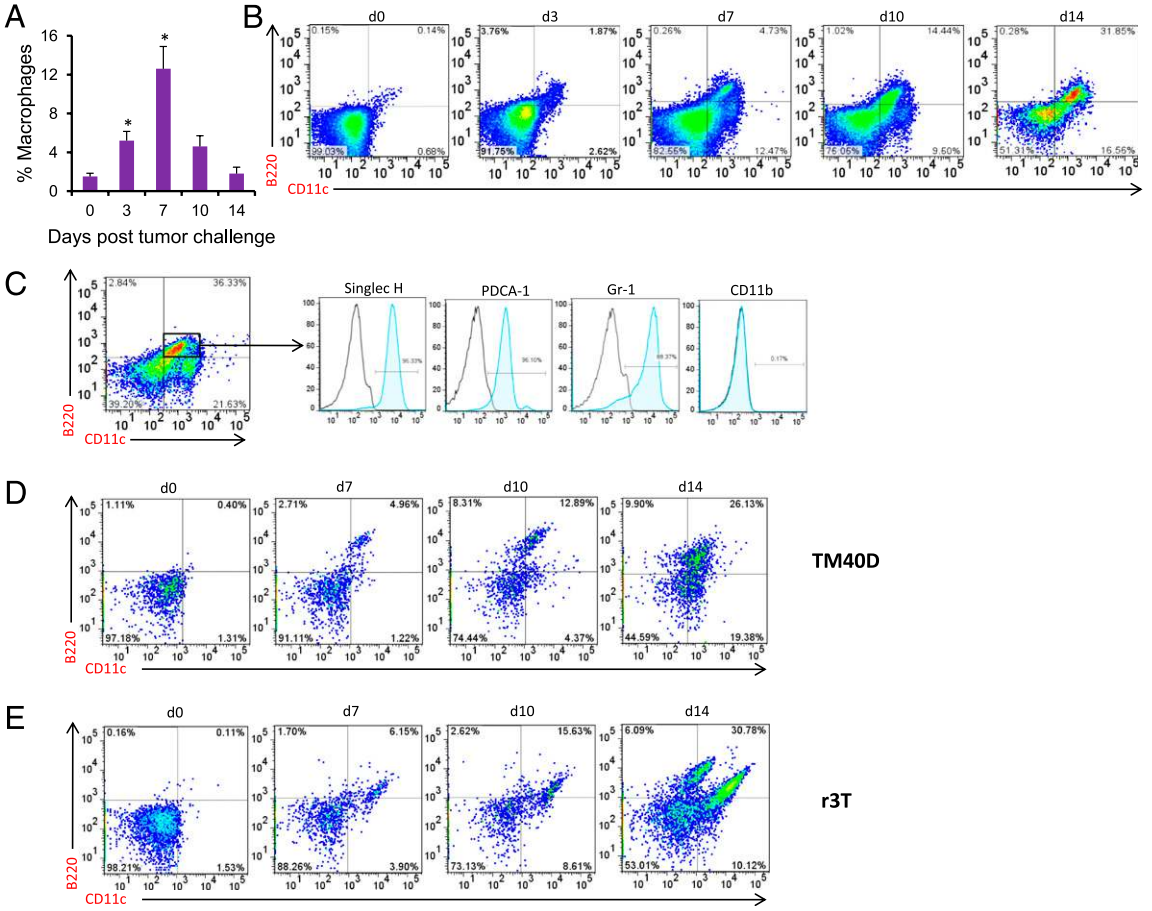

FIGURE 2. Numbers of pDC increase with increased dissemination of breast cancer to bone. (**A**) On days 3, 7, 10, and 14 following tumor cell injection, mice were sacrificed, and BM cells were isolated as described in *Materials and Methods*. The presence of macrophages was detected using anti-F4/80 and enumerated by flow cytometry. *$p < 0.05$, Student t test. (**B**) pDC were detected by staining with B220 and CD11c Abs and analyzed by flow cytometry. A representative data set from each time point is shown. (**C**) The presence of pDC ($B220^+CD11c^+$) was further confirmed with Singlec-H, PDCA-1, Gr-1, and CD11b Abs. Data are shown for mice 14 d posttumor challenge. (**D** and **E**) BALB/c and 129S mice were injected with TM40D and r3T cells, respectively, via the intracardiac route. pDC levels in BM were evaluated by flow cytometry using B220 and CD11c Abs on days 7, 10, and 14, as described in *Materials and Methods*. Representative data from each time point are shown. BM cells were isolated from six mice for every time point and were treated as individual samples. For each sample, the above-mentioned flow cytometry analysis was performed. This experiment was performed three times independently.

(fLuc) cells, which could have prevented their proliferation, 4T1 (fLuc) cells isolated from tumor-bearing mice were tested for their ability to bind to PDCA-1 Ab. Once breast cancer bone metastasis was established in mice, the animals were sacrificed, and BM cells were collected. Cells were stained for Abs to CD45 and PDCA-1. Because nonimmune cells do not express CD45, staining for PDCA-1 was detected among $CD45^-$ cells. The results clearly indicated an absence of PDCA-1 staining on $CD45^-$ cells. Further, to confirm that the $CD45^-$ cells that did not bind to PDCA-1 were indeed 4T1(fLuc) cells, these cells were sorted, and luciferase activity was determined in that population because the 4T1(fLuc) cells used in this study constitutively expressed firefly luciferase. A high luciferase count was detected, suggesting that a major fraction of $CD45^-PDCA\text{-}1^-$ cells were indeed breast cancer cells (Supplemental Fig. 2). This observation confirmed that in vivo breast cancer cells isolated from the bone microenvironment do not express PDCA-1, thus eliminating any direct effect of PDCA-1 Ab treatment on tumor growth and dissemination and validating its use for this study.

For further direct confirmation that pDC indeed play a vital role in breast cancer bone metastasis, a genetic mouse model lacking expression of IFN-αR ($IFNAR^{-/-}$) was used because these mice lack functional pDC (16, 17). A similar study in this model showed a dramatic reduction in the growth of breast cancer in $IFNAR^{-/-}$ mice compared with the syngeneic wild-type (WT) mice, thus confirming a role for pDC in promoting tumor growth and metastasis (Fig. 5F).

Micro-CT analysis of femur and tibia following PDCA-1 injection did not show the bone destruction seen in the naive and IgG-injected mice (Fig. 6A), which also correlated with fewer $TRAP^+$ osteoclasts in tibia (Fig. 6B). These results were further confirmed when, upon coculture of $CD4^+$ T cells and monocytes, the PDCA-1 group had significantly fewer osteoclasts compared with the naive and IgG groups (Fig. 6C). The decreased osteoclast numbers can be attributed to decreased amounts of osteoclast-inducing cytokines in mice treated with PDCA-1 Ab (Fig. 6D, Supplemental Fig. 3). Similar to the results observed in the PDCA-1 group, micro-CT analysis also revealed reduced bone destruction in tumor-challenged $IFNAR^{-/-}$ mice compared with the WT mice (Fig. 6E). Together, these data demonstrate that pDC enhance breast cancer bone metastasis.

Additionally, to rule out the possibility that the genetic background of $IFNAR^{-/-}$ mice (BALB/c) played a role in reduced tumor growth and osteolysis, a similar study was carried out in $IFNAR^{-/-}$ mice on a C57BL/6 background using an osteolytic cell line. The data clearly demonstrated that the genetic background of

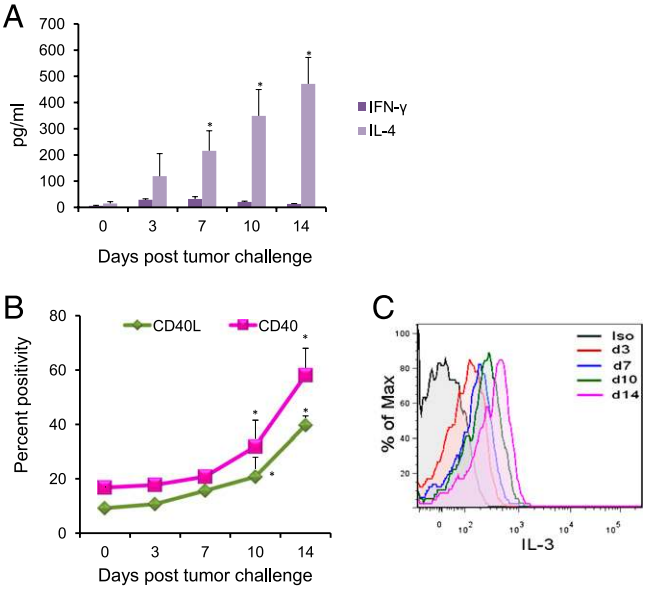

FIGURE 3. Increase in pDC is concomitant with the increase in Th2 cells. (**A**) Serum samples from mice were assayed for levels of IFN-γ and IL-4 by multiplex ELISA, per the manufacturer's instructions, on days 3, 7, 10, and 14 posttumor challenge. Results are expressed as picograms per milliliter of the respective cytokine ± SE ($n = 3$). (**B**) Cells stained for pDC and $CD4^+$ T cell markers were stained for CD40 and CD40L, respectively. Results are shown as percent positivity in the expression of these markers compared with control. (**C**) Cells isolated from BM were cultured in RPMI 1640 in the presence of 5 ng/ml PMA, 500 ng/ml ionomycin, and 1 μg/ml GolgiPlug protein transport inhibitor for 4 h. Cells were then stained with surface Abs to CD3 and CD4. Upon permeabilization, cells were stained with Ab to IL-3. The percentage of IL-3–secreting CD^+ T cells was analyzed by flow cytometry by intracellular staining. Data are a representative curve at each time point. For statistical analysis, six mice were included for each time point, and the experiment was repeated three times independently. $*p < 0.05$, Student t test.

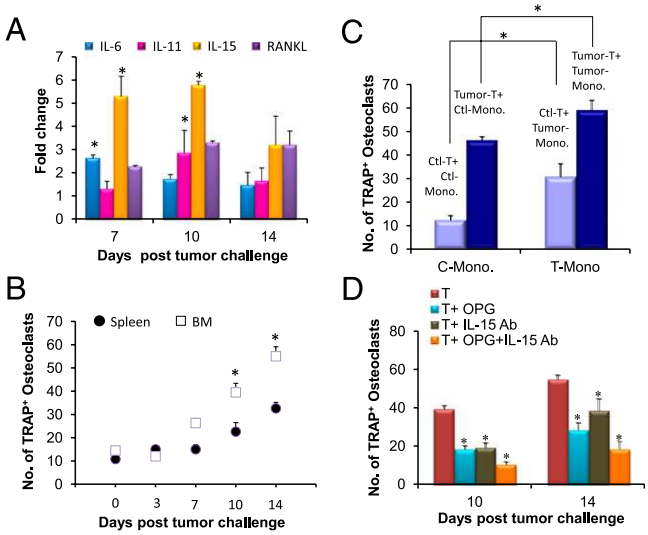

FIGURE 4. RANKL and IL-15 antagonist decrease osteoclast activity during bone metastasis of breast cancer cells. (**A**) RNA was isolated from BM $CD4^+$ T cells, and cDNA was synthesized and used in real-time RT-PCR analysis for IL-6, IL-11, IL-15, and RANKL. Data are presented as fold change in the expression of RNA compared with the control. (**B**) Monocytes and $CD4^+$ T cells isolated from BM and spleen were cocultured at a ratio of 1:100 for osteoclast differentiation. Cells with three or more nuclei were scored as osteoclasts following TRAP staining. (**C**) Monocytes isolated on day 14 from tumor-challenged mice were cocultured with $CD4^+$ T cells from either the tumor-challenged or the control mice for osteoclast differentiation. (**D**) On days 10 and 14, OPG or Ab to IL-15 was added to the cocultures of monocytes and $CD4^+$ T cells individually or in combination. After 10 d, TRAP staining was performed to detect the presence of osteoclasts. The above experiments were performed by isolating cells from six mice for each time point. The experiments were repeated three times independently. $*p < 0.05$, Student t test.

$IFNAR^{-/-}$ mice did not affect the results, because reduced tumor growth and osteolysis were also observed in $IFNAR^{-/-}$ mice on a C57BL/6 background (Supplemental Fig. 4).

Depletion of pDC restores a Th1 type immune response

We next analyzed the effect of pDC depletion on antitumor immunity. As expected, the numbers of pDC were markedly reduced in PDCA-1–injected mice compared with naive and IgG-injected mice (Fig. 7A). Decreased pDC levels resulted in an increase in Th1 cells, with a concomitant decrease in Th2 cells, as assessed by high IFN-γ and low IL-4 levels, respectively in the PDCA-1 Ab-injected group (Fig. 7B). However, in both naive and IgG Ab-injected mice, elevated Th2 cells were seen, as observed previously. Multiplex cytokine analysis further supported the immune profile, showing increased secretion of Th1-associated cytokines (Supplemental Fig. 3). Depletion of pDC also resulted in a decrease in myeloid-derived suppressor cells (MDSC) and Tregs compared with naive and IgG-injected mice (Fig. 7C, 7D). To determine the possible mechanism for reduced tumor growth in pDC-depleted mice, $CD8^+$ T cells were isolated and used in a cytotoxicity assay. Freshly isolated $CD8^+$ T cells from pDC-depleted mice exhibited significantly enhanced cytotoxicity compared with those from naive and IgG groups against 4T1 cells as the target population (Fig. 7E).

We also detected pDC levels in BM of WT and $IFNAR^{-/-}$ mice after tumor challenge. Unlike the elevated pDC levels observed in WT mice, $IFNAR^{-/-}$ mice did not exhibit such high pDC levels (Fig. 7F). This observation coincided with low pDC levels observed in the PDCA-1 Ab-injected group. Both of these groups of mice also showed drastically reduced breast cancer growth and bone metastasis.

Discussion

Studies using tissues from human breast cancer patients have documented infiltration of pDC at the periphery of tumor and at sites of metastasis (18, 19). pDC are also present in lymph nodes carrying breast cancer metastasis (20). However, the significance of this has not been clearly defined. Using metastatic models of breast cancer in immunocompetent mice, the present study initially established and then systematically defined these events connecting cancer growth and osteolysis through immune modulation. The results of these analyses clearly demonstrate that pDC play a key role in this vicious cascade.

From our studies, it is apparent that dissemination of breast cancer to the bone initiates the infiltration of macrophages (Fig. 2A), which produces an inflammatory response, resulting in the triggering of a pDC response (Fig. 2B). Although the signal that induces pDC accumulation has not been identified, it is possible that infiltration of macrophages to the site of invading cancer cells, as well as proliferating breast cancer cells in the bone microenvironment, may cause an increase in the production of Flt-3 ligand. Production of Flt-3 ligand, in turn, has been linked to inflammation in the bone postneoplastic breast cell infiltration (21).

Macrophage differentiation, growth, and chemotaxis are regulated by many growth factors, including CSF-1, GM-CSF, and IL-3, as well as several chemokines, including MCP-1 (CCL-2) and

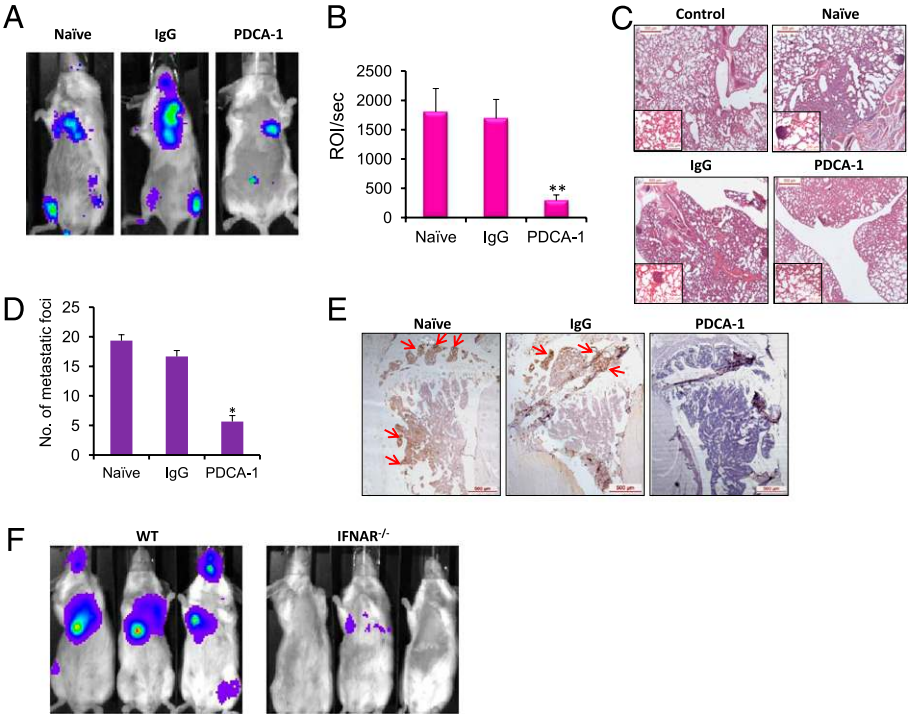

FIGURE 5. Depletion of pDC significantly reduces the growth of breast cancer cells in vivo. (**A**) Representative luciferase imaging of naive, IgG-treated, and PDCA-1–treated mice 12 d after tumor challenge. (**B**) Total luciferase counts from mice of each group 12 d posttumor challenge. (**C**) Paraffin section of lungs from naive, IgG-injected, and PDCA-1–injected mice were stained with H&E. A representative section from each group is shown (*insets*, original magnification ×20). Scale bars, 500 μm. (**D**) Breast cancer metastasis sites in the lungs were counted in naive, IgG-injected, and PDCA-1–injected mice. (**E**) Paraffin sections of tibia from naive, IgG-treated, and PDCA-1–treated mice were stained with cytokeratin-8 Ab. Arrows indicate the presence of breast cancer cells. Scale bars, 500 μm. (**F**) Representative luciferase imaging of 4T1(fLuc) cell-challenged WT and IFNAR$^{-/-}$ mice (BALB/c background) 12 d posttumor challenge. Depletion of pDC was performed twice independently. Three mice were included in naive, IgG, and PDCA-1 groups for each time point. *$p < 0.05$, **$p < 0.01$, Student *t* test.

RANTES (CCL5). MCP-1 overexpression was reported in many cancers, including breast cancer (22–25). Similarly, a significant increase in RANTES was also reported in BM microenvironment of multiple myeloma patients (26). The results of multiplex analysis indicated a significant increase in MCP-1, RANTES, IL-3, and IL-6, suggesting a probable role for these cytokines and growth factors in macrophage infiltration (Supplemental Fig. 1). The levels of proinflammatory cytokines were significantly reduced following pDC depletion, which correlated with an absence of bone metastasis. In contrast, IP-10, a potent inhibitor of both angiogenesis and tumor growth in the bone in vivo (27, 28), was upregulated in pDC-depleted mice (Supplemental Fig. 3), thus supporting the importance of these molecules in suppressing bone metastasis in these mice.

Another notable finding of the current study is elevated levels of pDC Tregs, Th2 cells, and MDSC in the BM compared with the spleen suggesting that the suppressive immune response is polarized more in the BM than in the spleen (data not shown). Because pDC reside mainly in the bone, it was not surprising to note greater levels in the BM; however, a striking discovery in the current study was the prevalence of an increasing pDC population as cancer growth progressed in the bone. pDC activation of CD4$^+$ T cells was

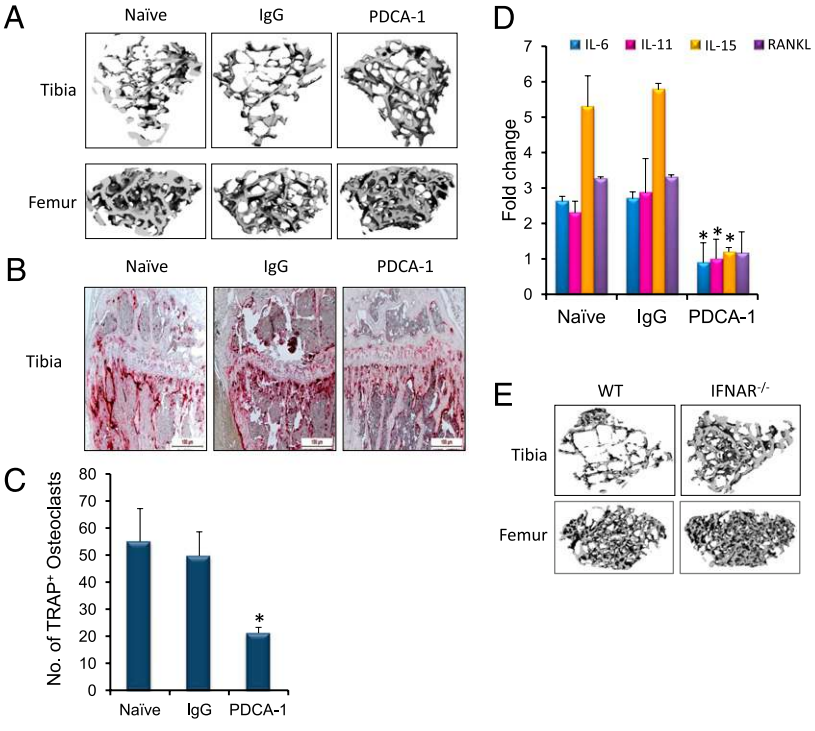

FIGURE 6. Decreased numbers of osteoclasts results in the absence of bone destruction in pDC-depleted mice. (**A**) Twelve days posttumor challenge, tibia and femur from naive and IgG- and PDCA-1–treated mice were subjected to micro-CT analysis. (**B**) Paraffin sections of tibia from naive, IgG-injected, and PDCA-1–injected mice were stained with TRAP 12 d after tumor challenge to detect osteoclasts. Scale bars, 100 μm. (**C**) On day 12 posttumor challenge, monocytes and CD4$^+$ T cells from naive and IgG- and PDCA-1 Ab-injected mice were cocultured to assay osteoclast numbers. (**D**) cDNA from CD4$^+$ T cells of naive and IgG- and PDCA-1 Ab-treated mice were used to detect the levels of IL-6, IL-11, IL-15, and RANKL by real-time RT-PCR. Data are presented as a fold change in expression of RNA compared with the control. (**E**) Micro-CT analysis of tibia and femur from WT and IFNAR$^{-/-}$ mice 12 d posttumor challenge. Data are from three mice for each group. The experiments were repeated twice separately. *$p < 0.05$, Student *t* test.

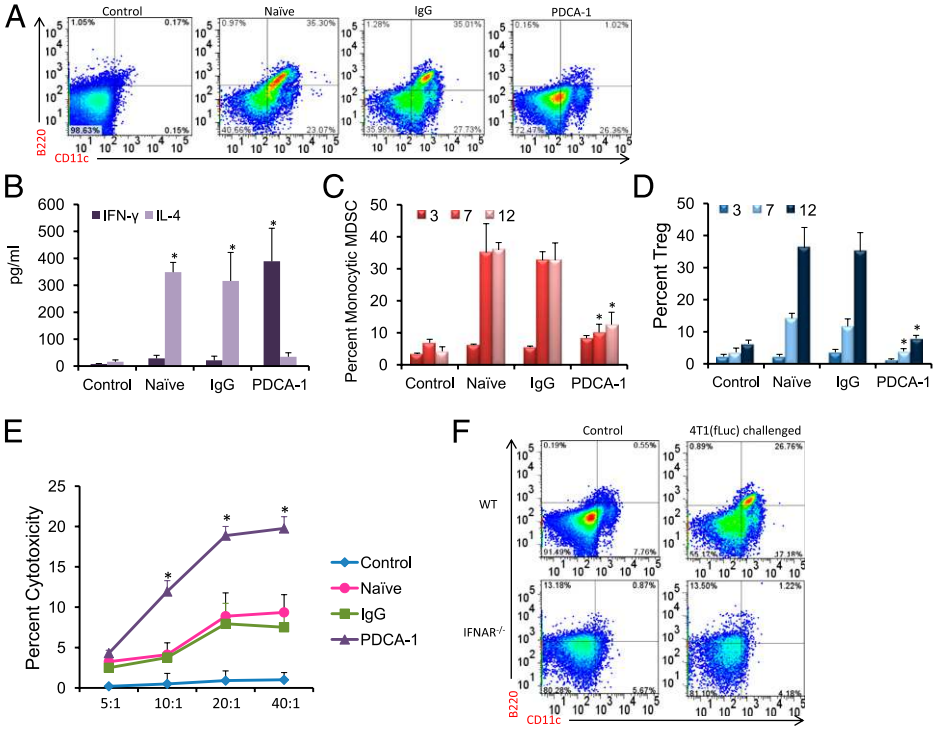

FIGURE 7. Depletion of pDC skews the immune response toward Th1 and results in decreased immunosuppression. (**A**) pDC were detected in BM from naive and IgG- and PDCA-1 Ab-injected mice 12 d posttumor challenge. A representative image from the three groups is presented. (**B**) IFN-γ and IL-4 levels were measured as described previously. (**C**) The numbers of monocytic MDSC ($CD11b^+Gr\text{-}1^+Ly6C^+Ly6G^{lo}$) in the BM after pDC depletion were enumerated by flow cytometry. (**D**) The presence of Tregs was detected by staining BM cells from control and IgG- and PDCA-1 Ab-treated mice. (**E**) $CD8^+$ T cells isolated from the BM of IgG- and PDCA-1–treated animals 3 d posttumor challenge were used as the effector population, and 4T1(fLuc) cells were used as the target population. A cytotoxicity assay was carried out using a commercially available kit. (**F**) The presence of pDC was detected in BM from WT and $IFNAR^{-/-}$ mice 12 d posttumor challenge. Mice with no tumor challenge were included as the control group. A representative image for each group, showing the percentage of pDC, is presented. The flow cytometry and cytotoxicity assay data are from three mice for each group and for each time point. The experiments were repeated twice independently. $*p < 0.05$, Student t test.

correlated with higher CD40 expression on pDC and higher CD40L expression on $CD4^+$ T cells, along with increased IL-3 production by $CD4^+$ T cells. This ligation was maintained throughout the period of progressive cancer burden and bone destruction, suggesting that constant stimulation of $CD4^+$ T cells by pDC is critical for skewing and maintaining the immune response toward a Th2 phenotype (29, 30). Concomitant with this effect, the osteolytic cytokines IL-3, IL-6, IL-11, and IL-15 were maintained at elevated levels (31, 32).

Skewing of the immune response toward the Th2 phenotype was associated with a decreased Th1 response. Elevated Th2-associated cytokines IL-13, IL-4, and IL-5, along with low levels of Th1 cytokines, such as IP-10 and IFN-γ (Fig. 3, Supplemental Fig. 3), further maintained Th2 polarization. At the initial stage of cancer dissemination (notably days 3 and 7), there was an initial spike in Th1 cells (Fig. 3). This observation suggests that, although a significant Th1 response was not noted during the progressive stages of breast cancer dissemination, a notable increase in Th1 cells during the first few days caused an initial influx of antitumor activity-inducing immune effector cells, which may have been dampened by a gradual increase in pDC and Th2 cells and associated cytokine production, facilitating immunosuppression, tumor growth, and osteolysis.

It was not surprising to observe increased levels of both Tregs and MDSC in the bone microenvironment. Both of these immunosuppressive cells are known to be upregulated in the presence of IL-10 and TGF-β (33). Interestingly, activated Tregs were noted even at a late stage of the disease, when the overall host immune response may have been greatly dampened due to increased tumor burden. Recent studies showed that MDSC induce immune suppression and allow the progression of several cancers, including breast cancer, and a reduction in MDSC significantly delays primary tumor growth (34–37).

The significance of high pDC numbers and a shift in T cell homeostasis in promoting tumor growth, immunosuppression, and osteolytic bone damage was further confirmed by depletion of the pDC population prior to tumor challenge. Dampening of the pDC response resulted in a greater decrease of tumor growth in the bone, as well as in other metastatic sites, including lungs and liver. The results indicated a shift from a Th2 to a Th1 immune response following pDC depletion, as evidenced by an increase in IL-12 production (Supplemental Fig. 3) and activated Th1 cells. A cytotoxicity assay using $CD8^+$ T cells isolated from pDC-depleted mice further confirmed a direct effect on both the reversal to Th1 polarization and antitumor activity in the bone and in visceral tissues, along with an increase in IFN-γ levels. Thus, it remains possible that augmentation of antitumor immunity may be achieved in breast cancer patients by depleting pDC accumulation (18, 19).

Coupled with other cancer immunotherapy strategies, such as active immune response through tumor Ag-specific vaccines or treatments aimed at nonspecific activation of immune effectors by passive immunotherapy, including GM-CSF and IL-2 therapies, pDC-depletion therapy is likely to promote an augmented antitumor effect and extend survival. A remarkable decrease in the production of osteolytic cytokines following pDC depletion also strongly suggests that incorporation of this unique axis into therapy regimens will improve bone remodeling significantly and decrease progressive bone loss in patients with breast cancer.

Acknowledgments

We thank Enid Keyser for technical assistance with flow cytometry and sorting and the Analytical and Preparative Cytometry Facility (supported by National Institutes of Health Grant P30 AR48311) of the Comprehensive Arthritis, Musculoskeletal and Autoimmunity Center at the University of Alabama at Birmingham (UAB). Noninvasive imaging was carried out at UAB's Small Animal Imaging facility. Bone histomorphometry and micro-CT analyses were performed at UAB's Bone Histomorphometry Core and Small Animal Bone Phenotyping Core, respectively. Flow cytometry analysis was performed at the UAB Center for AIDS Research Core facility.

Disclosures

The authors have no financial conflicts of interest.

References

1. Lippman, M. E. 2011. Breast cancer. In *Harrison's Principles of Internal Medicine*. *Part 7*. 18th Ed. Dan L. Longo, Anthony Fauci, Dennis Kasper, Stephen Hauser, J. Larry Jameson, and Joseph Loscalzo, eds. McGraw-Hill, New York, p. 516–523.
2. Roodman, G. D. 2004. Mechanisms of bone metastasis. *N. Engl. J. Med.* 350: 1655–1664.
3. Mundy, G. R. 2002. Metastasis to bone: causes, consequences and therapeutic opportunities. *Nat. Rev. Cancer* 2: 584–593.
4. Takayanagi, H. 2009. Osteoimmunology and the effects of the immune system on bone. [Published erratum appears in 2010 *Nat. Rev. Rheumatol.* 6: 4.] Nat. Rev. Rheumatol. 5: 667–676.
5. Kong, Y. Y., and J. M. Penninger. 2000. Molecular control of bone remodeling and osteoporosis. *Exp. Gerontol.* 35: 947–956.
6. Bussard, K. M., C. V. Gay, and A. M. Mastro. 2008. The bone microenvironment in metastasis; what is special about bone? *Cancer Metastasis Rev.* 27: 41–55.
7. Cao, Q., W. Cai, G. Niu, L. He, and X. Chen. 2008. Multimodality imaging of IL-18–binding protein-Fc therapy of experimental lung metastasis. *Clin. Cancer Res.* 14: 6137–6145.
8. Bernt, K. M., S. Ni, A. T. Tieu, and A. Lieber. 2005. Assessment of a combined, adenovirus-mediated oncolytic and immunostimulatory tumor therapy. *Cancer Res.* 65: 4343–4352.
9. Chen, Y., and S. R. Rittling. 2003. Novel murine mammary epithelial cell lines that form osteolytic bone metastases: effect of strain background on tumor homing. *Clin. Exp. Metastasis* 20: 111–120.
10. Bailey-Bucktrout, S. L., S. C. Caulkins, G. Goings, J. A. Fischer, A. Dzionek, and S. D. Miller. 2008. Cutting edge: central nervous system plasmacytoid dendritic cells regulate the severity of relapsing experimental autoimmune encephalomyelitis. *J. Immunol.* 180: 6457–6461.
11. Chanda, D., T. Isayeva, S. Kumar, J. A. Hensel, A. Sawant, G. Ramaswamy, G. P. Siegal, M. S. Beatty, and S. Ponnazhagan. 2009. Therapeutic potential of adult bone marrow-derived mesenchymal stem cells in prostate cancer bone metastasis. *Clin. Cancer Res.* 15: 7175–7185.
12. Erlebacher, A., and R. Derynck. 1996. Increased expression of TGF-beta 2 in osteoblasts results in an osteoporosis-like phenotype. *J. Cell Biol.* 132: 195–210.
13. duPre', S. A., D. Redelman, and K. W. Hunter, Jr. 2008. Microenvironment of the murine mammary carcinoma 4T1: endogenous IFN-gamma affects tumor phenotype, growth, and metastasis. *Exp. Mol. Pathol.* 85: 174–188.
14. Palmqvist, P., P. Lundberg, E. Persson, A. Johansson, I. Lundgren, A. Lie, H. H. Conaway, and U. H. Lerner. 2006. Inhibition of hormone and cytokine-stimulated osteoclastogenesis and bone resorption by interleukin-4 and interleukin-13 is associated with increased osteoprotegerin and decreased RANKL and RANK in a STAT6-dependent pathway. *J. Biol. Chem.* 281: 2414–2429.
15. Rissoan, M.-C., V. Soumelis, N. Kadowaki, G. Grouard, F. Briere, R. de Waal Malefyt, and Y. J. Liu. 1999. Reciprocal control of T helper cell and dendritic cell differentiation. *Science* 283: 1183–1186.
16. Muller, A. J., M. D. Sharma, P. R. Chandler, J. B. Duhadaway, M. E. Everhart, B. A. Johnson, III, D. J. Kahler, J. Pihkala, A. P. Soler, D. H. Munn, et al. 2008. Chronic inflammation that facilitates tumor progression creates local immune suppression by inducing indoleamine 2,3 dioxygenase. *Proc. Natl. Acad. Sci. USA* 105: 17073–17078.
17. Asselin-Paturel, C., G. Brizard, K. Chemin, A. Boonstra, A. O'Garra, A. Vicari, and G. Trinchieri. 2005. Type I interferon dependence of plasmacytoid dendritic cell activation and migration. *J. Exp. Med.* 201: 1157–1167.
18. Ferrari, S., F. Malugani, B. Rovati, C. Porta, A. Riccardi, and M. Danova. 2005. Flow cytometric analysis of circulating dendritic cell subsets and intracellular cytokine production in advanced breast cancer patients. *Oncol. Rep.* 14: 113–120.
19. Treilleux, I., J. Y. Blay, N. Bendriss-Vermare, I. Ray-Coquard, T. Bachelot, J. P. Guastalla, A. Bremond, S. Goddard, J. J. Pin, C. Barthelemy-Dubois, and S. Lebecque. 2004. Dendritic cell infiltration and prognosis of early stage breast cancer. *Clin. Cancer Res.* 10: 7466–7474.
20. Horny, H. P., A. C. Feller, H. A. Horst, and K. Lennert. 1987. Immunocytology of plasmacytoid T cells: marker analysis indicates a unique phenotype of this enigmatic cell. *Hum. Pathol.* 18: 28–32.
21. Cohen, P. A., G. K. Koski, B. J. Czerniecki, K. D. Bunting, X. Y. Fu, Z. Wang, W. J. Zhang, C. S. Carter, M. Awad, C. A. Distel, et al. 2008. STAT3- and STAT5-dependent pathways competitively regulate the pan-differentiation of CD34pos cells into tumor-competent dendritic cells. *Blood* 112: 1832–1843.
22. Fujimoto, H., T. Sangai, G. Ishii, A. Ikehara, T. Nagashima, M. Miyazaki, and A. Ochiai. 2009. Stromal MCP-1 in mammary tumors induces tumor-associated macrophage infiltration and contributes to tumor progression. *Int. J. Cancer* 125: 1276–1284.
23. Ksiazkiewicz, M., E. Gottfried, M. Kreutz, M. Mack, F. Hofstaedter, and L. A. Kunz-Schughart. 2010. Importance of CCL2-CCR2A/2B signaling for monocyte migration into spheroids of breast cancer-derived fibroblasts. *Immunobiology* 215: 737–747.
24. Lazar, M., J. Sullivan, G. Chipitsyna, T. Aziz, A. F. Salem, Q. Gong, A. Witkiewicz, D. T. Denhardt, C. J. Yeo, and H. A. Arafat. 2010. Induction of monocyte chemoattractant protein-1 by nicotine in pancreatic ductal adenocarcinoma cells: role of osteopontin. *Surgery* 148: 298–309.
25. Mishra P., D. Banerjee, and A. Ben-Baruch. 2011. Chemokines at the crossroads of tumor-fibroblast interactions that promote malignancy. *J. Leukoc. Biol.* 89: 31–39.
26. Cao, Y., T. Luetkens, S. Kobold, Y. Hildebrandt, M. Gordic, N. Lajmi, S. Meyer, K. Bartels, A. R. Zander, C. Bokemeyer, et al. 2010. The cytokine/chemokine pattern in the bone marrow environment of multiple myeloma patients. *Exp. Hematol.* 38: 860–867.
27. Angiolillo, A. L., C. Sgadari, D. D. Taub, F. Liao, J. M. Farber, S. Maheshwari, H. K. Kleinman, G. H. Reaman, and G. Tosato. 1995. Human interferon-inducible protein 10 is a potent inhibitor of angiogenesis in vivo. *J. Exp. Med.* 182: 155–162.
28. Dufour, J. H., M. Dziejman, M. T. Liu, J. H. Leung, T. E. Lane, and A. D. Luster. 2002. IFN-gamma-inducible protein 10 (IP-10; CXCL10)-deficient mice reveal a role for IP-10 in effector T cell generation and trafficking. *J. Immunol.* 168: 3195–3204.
29. Chaperot, L., I. Perrot, M. C. Jacob, D. Blanchard, V. Salaun, V. Deneys, S. Lebecque, F. Brière, J. C. Bensa, and J. Plumas. 2004. Leukemic plasmacytoid dendritic cells share phenotypic and functional features with their normal counterparts. *Eur. J. Immunol.* 34: 418–426.
30. Martín-Gayo, E., E. Sierra-Filardi, A. L. Corbí, and M. L. Toribio. 2010. Plasmacytoid dendritic cells resident in human thymus drive natural Treg cell development. *Blood* 115: 5366–5375.
31. Lebre, M. C., S. L. Jongbloed, S. W. Tas, T. J. Smeets, I. B. McInnes, and P. P. Tak. 2008. Rheumatoid arthritis synovium contains two subsets of CD83−DC−LAMP− dendritic cells with distinct cytokine profiles. *Am. J. Pathol.* 172: 940–950.
32. Nasrazadani, A., and C. L. Van Den Berg. 2011. c-Jun N-terminal Kinase 2 Regulates Multiple Receptor Tyrosine Kinase Pathways in Mouse Mammary Tumor Growth and Metastasis. *Genes Cancer* 2: 31–45.
33. Jia, W., C. Jackson-Cook, and M. R. Graf. 2010. Tumor-infiltrating, myeloid-derived suppressor cells inhibit T cell activity by nitric oxide production in an intracranial rat glioma + vaccination model. *J. Neuroimmunol.* 223: 20–30.
34. Sinha, P., V. K. Clements, S. K. Bunt, S. M. Albelda, and S. Ostrand-Rosenberg. 2007. Cross-talk between myeloid-derived suppressor cells and macrophages subverts tumor immunity toward a type 2 response. *J. Immunol.* 179: 977–983.
35. Corzo, C. A., T. Condamine, L. Lu, M. J. Cotter, J. I. Youn, P. Cheng, H. I. Cho, E. Celis, D. G. Quiceno, T. Padhya, et al. 2010. HIF-1α regulates function and differentiation of myeloid-derived suppressor cells in the tumor microenvironment. *J. Exp. Med.* 207: 2439–2453.
36. Cao, M., Y. Xu, J. I. Youn, R. Cabrera, X. Zhang, D. Gabrilovich, D. R. Nelson, and C. Liu. 2011. Kinase inhibitor Sorafenib modulates immunosuppressive cell populations in a murine liver cancer model. *Lab. Invest.* 91: 598–608.
37. Fujita, M., G. Kohanbash, W. Fellows-Mayle, R. L. Hamilton, Y. Komohara, S. A. Decker, J. R. Ohlfest, and H. Okada. 2011. COX-2 blockade suppresses gliomagenesis by inhibiting myeloid-derived suppressor cells. *Cancer Res.* 71: 2664–2674.